Atomic Transfer in Halogen-Bonded Complexes Mediated by Polarizing Environments: Mimicking Intra- and Intermolecular Effects in a Series of Cocrystals of N-Bromosaccharin with Pyridines

Emmanuel Aubert, Irène Nicolas, Olivier Jeannin, Marc Fourmigué, Enrique Espinosa

Atomic transfer in halogen-bonded complexes mediated by polarizing environments: Mimicking intra- and inter-molecular effects in a series of cocrystals of N-bromosaccharin with pyridines

Emmanuel Aubert,[a] Irène Nicolas,[b] Olivier Jeannin,[b] Marc Fourmigué[b,*] and Enrique Espinosa,[a,*]

[a] *Université de Lorraine, CNRS, CRM2 (Laboratoire de Cristallographie, Résonance Magnétique et Modélisations), UMR 7036 , F-54000 Nancy (France)*

[b] *Université de Rennes, CNRS, ISCR (Institut des Sciences Chimiques de Rennes), UMR 6226, F-35000 Rennes (France)*

Abstract.

The good halogen bond donor N-bromo-saccharin (NBrSac) has been co-crystallized with four *para*-substituted pyridines (PyX) as good halogen bond acceptors of different strengths (PyCN, $PyCF_3$, $PyCO_2Me$ and PyMe). Their crystal structures have been determined and permitted to observe the formation of adducts with a significantly weakened N_{Sac}•••Br bonding interaction with respect to the NBrSac donor and the formation of a strong Br•••N_{Py} interaction. The topological properties at the N_{Sac}•••Br•••N_{Py} bond critical points (BCPs) of the adducts frozen at experimental geometries indicate the increasing strength of the studied acceptors along the series PyCN < $PyCF_3$ < $PyCO_2Me$ < PyMe, correlating with the structural distances and the deeper negative MESP values in the individual molecules. The polarizability calculated in individual molecules clearly points out the atomic dipole moments of the N_{Sac}, Br and N_{Py} atoms, increasing in magnitude within the adducts and demonstrating their sensitivity to external electric fields mimicking molecular environments. In order to explore the effect of polarizing environments on the N_{Sac}•••Br•••N_{Py} halogen bonding motif, an external electric field has been applied ($-40\times10^{-4} < \varepsilon < 100\times10^{-4}$ a.u.) to adducts extracted from experimental geometries with all atoms frozen except Br, which has been optimized as a function of ε. It has been shown that an effective electric field ranging from 1.28 to 2.96 GV m^{-1} is necessary to recover the experimental position of the Br-atom in the adducts (from the one calculated in gas-phase optimization), providing an evaluation of the effect of the crystalline environment. At any investigated geometry (*i.e.*, within the full range of applied fields), the adducts exhibit a significant covalence degree at both donor and acceptor sides (measured by $1 < |V|/G < 2$), in

addition to a non-negligible delocalization index $DI(N_{Sac}|N_{Py})$ in the range 0.085-0.099. These features indicate that the adducts should be considered as a unique molecular entity rather than two, while pointing an assembly with a small but non-negligible contribution of a three-center four-electrons interaction. The formal border of the halogen atom transfer between donor and acceptor moieties is stablished by the topological magnitudes of ρ and $|V|/G$ at both bond critical points, as well as that of *DI*, which all balance almost simultaneously in donor and acceptor regions. The position of the halogen atom within the adduct is straightforwardly driven by the external polarization induced by ε, permitting to control the significant variation of the dipole moment of the adducts.

Introduction

It is now well established that halogen bonding (XB) can be used as an efficient tool to control and organize condensed phases into desired structures,[1] with an efficiency that now compares with hydrogen bonding (HB). XB interactions can be as strong as and even more directional than HB.[2] These studies have provided a broad palette of 'tectons' or 'synthons',[3,4] most often based on cocrystal formation.[5,6] Interest for XB co-crystals[7,8] has also reached the pharmaceutical area since key properties of a solid active pharmaceutical Ingredient (API), such as solubility, dissolution rate and stability, can be deeply modified in a co-crystal.[9] Most examples rely in this domain on hydrogen bonded systems, where the API acts either as hydrogen bond donor or acceptor. In many instances, the question arises on the real nature of such HB systems, as many cocrystals have been prepared through strong hydrogen bonds, notably between a carboxylic acid and an N-heterocyclic hydrogen-bond acceptor. Depending on the exact position of the hydrogen atom between the oxygen and nitrogen ones, the compound can be described either as a neutral cocrystal or as a salt. The distinction has important consequences on the chemical (solvate) or stoichiometric composition of the compounds, since neutral cocrystals proved to provide more predictable compositions and structures than the salts.[10] We have recently investigated to which extend a similar distinction could be found in *halogen-bonded* rather than hydrogen-bonded systems, as illustrated in Scheme 1a, where the exact position of an iodine atom in a XB system could similarly control the state of a XB system, either a neutral cocrystal or a zwitterionic halonium salt.[11]

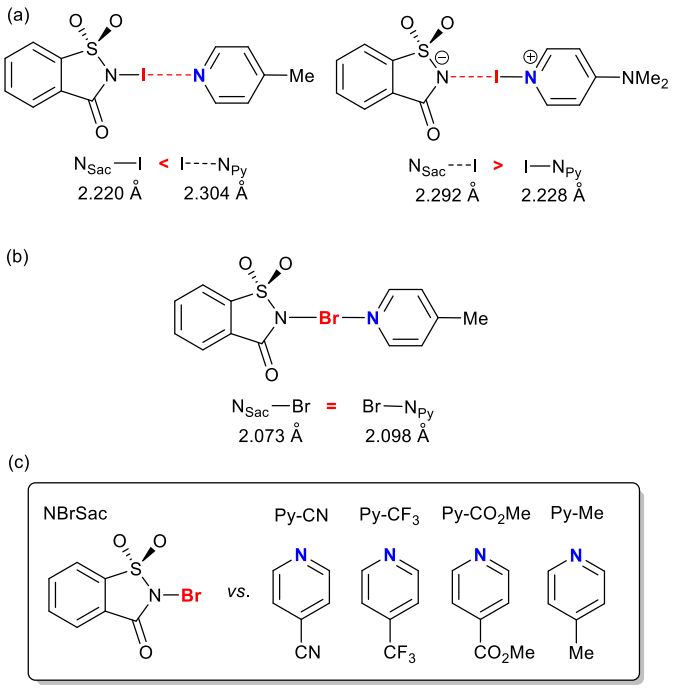

Scheme 1 Halogen bonded systems involving NISac and NBrSac

Accordingly, we have highlighted the efficient halogen bond donor character of N–iodosaccharin (NISac),[12] and demonstrated that with electron-rich Lewis bases such as 4-dimethylaminopyridine (abbreviated as $PyNMe_2$), the 1:1 NISac•$PyNMe_2$ adduct could be better described under its ionic form, that is a saccharinate anion halogen bonded to the corresponding N-iodopyridinium.[11] Under this description, the N-iodopyridinium cation acts now as the halogen bond donor. Such halonium salts are essentially know in symmetrical systems such as the archetypal $[Py–I–Py]^+$ cation,[13,14] or the recently investigated $[NSac•••I•••NSac]^-$ anionic systems.[15] In a recent review, Rissanen and Haukka also described these very strong halogen bonds as coordinative halogen bonds, by analogy with very similar structures found in corresponding d^{10}, Cu^+, Ag^+ and Au^+ linear complexes.[16] They also observed that the reduction ratio for the N•••X bond was even shorter in the bromonium than in the iodonium salts (RR_{NBr} = 0.63, RR_{NI} = 0.65). This result is at first sight relatively surprising as halogen bonding with bromine is usually observed to be weaker than with iodine. Accordingly, we decided to extend our work on NISac to the analogous N-bromosaccharin (NBrSac) adducts with pyridines, in order to evaluate how the neutral-to-ionic evolution is modified in bromine-based systems. Our first results with electron-rich pyridines such as 4-dimethylaminopyridine did not afford the expect co-crystal but rather a bromination product of Py-NMe_2 (in *meta* position). On the other hand, 4-picoline (noted PyMe) gave the 1:1 adduct NBrSac•PyMe,[17] where the bromine atom of NBrSac was found to be displaced toward the picoline, almost at a

median position between the two nitrogen atoms (Scheme 1b), at variance with the analogous iodine derivative, NISac•PyMe, where the N_{Sac}•••I and I•••N_{PyMe} distances amount to 2.223(4) and 2.301(4) Å respectively. Also, a stronger charge transfer to the picoline is found for the bromine (+0.27 |e|) than for the iodine (+0.18 |e|) system. This inversion of halogen bond strength between I and Br was analyzed as the consequence of a strong covalent character of the interaction in these adducts, in line with the strength of covalent N–Br and N–I bonds.

In order to investigate these effects in more details, we decided to expand these series of NBrSac adducts and describe here our results with three electron-poor pyridines, substituted in *para* position with electron-withdrawing groups R = CO_2Me, CF_3, CN (Scheme 1c), noted respectively in the following $PyCO_2Me$, $PyCF_3$ and PyCN. We report here the crystallization and the crystal structure of these three adducts, namely NBrSac•$PyCO_2Me$, NBrSac•$PyCF_3$ and NBrSac•PyCN, and compare them with the reported 4-methylpyridine adduct, NBrSac•PyMe.[17] This extensive series complements the reported structures involving NBrSac, namely NBrSac itself, a 2:1 adduct with pyrazine formulated as $(NBrSac)_2$(pyrazine),[12] and a large series of NBrSac adducts with various pyridine N-oxides.[18] The analysis of the electronic characteristics of these XB systems will be performed by a combination of theoretical calculations on the isolated molecules and XB-adducts as well as on the crystalline structures (periodic calculations), in order to evaluate the nature and strength of the interaction, as well as its sensitivity to external constraints, mimicked here by the application, within the calculations, of an external electric field along the N_{Sac}•••Br•••N_{Py} axis.

Results and Discussion

Syntheses and structures. All NBrSac adducts were prepared by vapor diffusion of hexane over a filtered solution of NBrSac with two equivalents of the 4-substituted pyridine dissolved in the appropriated solvent. The 1:1 composition of the crystals was confirmed by NMR, elemental analysis and single crystal X-ray structure determinations (Figure 1). The halogen bond interaction (Table 1) is in every case highly linear and short, with a Br•••N_{Py} distance (2.25–2.10) much shorter than the sum of the Br (1.85 Å) and N (1.55 Å) van der Waals radii (3.40 Å). The reduction ratio varies from 0.66 with the electron poor 4-cyanopyridine to 0.62 with 4-picoline. The strength of the halogen bond interaction can be evaluated not only from this evolution of the Br•••N_{Py} distance, but also from the total N_{Sac}•••N_{Py} distance, which appears here to shorten together with the Br•••N_{Py} distance, the indication of an increasing ionic

contribution to the strongest interactions. The evolution within the whole pyridine series, including the reported pyrazine adduct, parallels that reported for pyridine derivatives acting as halogen bond acceptor toward I_2, as described by Laurence and Graton with their pK_{BI2} scale.[19]

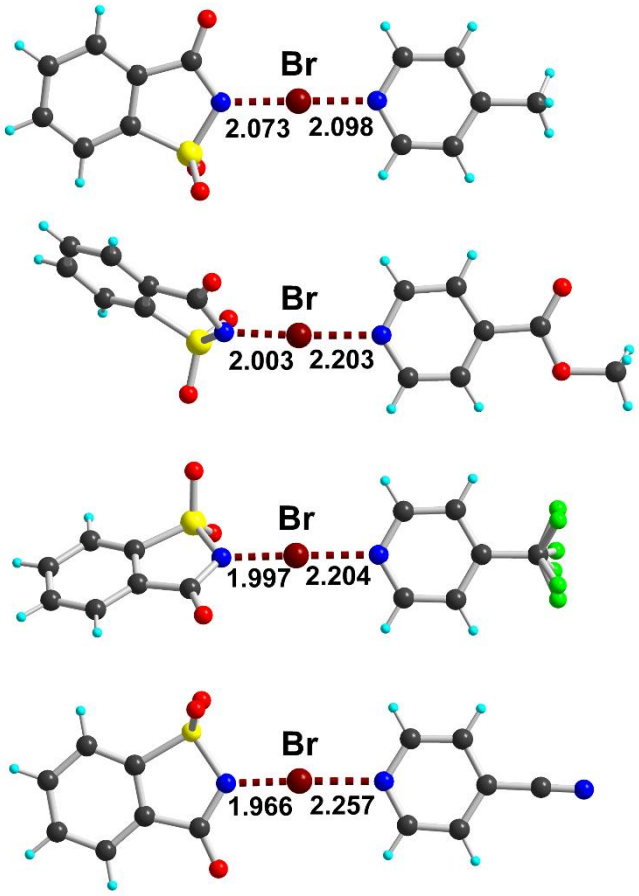

Figure 1. X-ray structures of the bimolecular adducts of NBrSac with, from top to bottom, 4-picoline, methylisonicotinate, 4-trifluoromethylpyridine and 4-cyanopyridine.

Table 1. Relevant distances and angles (Å, °) of the N_{Sac}•••Br•••N_{Py} halogen bond in the co-crystals with NBrSac. d_1 = N_{Sac}•••Br distance, d_2 = Br•••N_{Py} distance, $d_1 + d_2$ = N_{Sac}•••N_{Py} distance (the interaction is very close to linear). The dihedral angle is calculated between the five-membered ring of the saccharin and the pyridine ring.

	d_1 (N_{Sac}•••Br)	d_2 (Br•••N_{Py})	$d_1 - d_2$	Angle N_{Sac}•••Br•••N_{Py}	$d_1 + d_2$ (N_{Sac}•••N_{Py})	Dihedral angle	Ref.
PyMe	2.073(6)	2.098(6)	–0.025	178.74(8)	4.171(12)	14.56(7)	17

$PyCO_2Me$	2.003(1)	2.203(1)	–0.200	176.03(6)	4.203(2)	68.62(5)	this work
$PyCF_3$	1.997(3)	2.204(2)	–0.207	177.46(9)	4.200(4)	47.55(8)	this work
PyCN	1.966(1)	2.257(1)	–0.291	177.00(5)	4.222(2)	5.04(4)	this work
Pyrazine[a]	1.906(1)	2.410(1)	–0.504	175.22(6)	4.316(2)	61.40(4)	12

[a] Stoichiometry of two NBrSac for one pyrazine.

Electronic structures of the isolated molecules. Gas-phase calculations of XB donor and acceptors considered separately were carried at optimized geometries to analyze their electronic capabilities to form complexes (Table 2).

Table 2. Electronic properties of Br and N_{Py} atoms (PBEPBE D2 aug-cc-pVTZ calculations) in donor and acceptor monomers: Integrated net electronic charge $Q(e)$, $\rho(eÅ^{-3})$, $L = -\nabla^2\rho$ $(eÅ^{-5})$ and L/ρ $(Å^{-2})$ at CD and CC sites, and $MESP_{max}$ and $MESP_{min}$ (kcal/mol) on the ρ = 0.002 a.u. iso-density surface.

	Br atom in **NBrSac**	N_{Py} atom in **PyCN**	N_{Py} atom in **$PyCF_3$**	N_{Py} atom in **$PyCO_2Me$**	N_{Py} atom in **PyMe**
Q(Br) or $Q(N_{Py})$	0.2884	−1.0368	−1.0448	−1.0462	−1.0594
$MESP_{max}$(Br) or $MESP_{min}(N_{Py})$	+41.91	−31.31	−34.28	−38.18	−43.35
ρ_{CD}(Br) or $\rho_{CC}(N_{Py})$	28.307	3.977	3.972	3.970	3.933
L_{CD}(Br) or $L_{CC}(N_{Py})$	−1763.3	+62.4	+62.3	+62.3	+60.9
$(L/\rho)_{CD}$(Br) or $(L/\rho)_{CC}(N_{Py})$	−62.3	+15.7	+15.7	+15.7	+15.5

Electrophilic and nucleophilic regions in donor (NBrSac) and acceptors (PyX; X = CN, CF_3, CO_2Me, Me) molecules are shown by the plot of the molecular electrostatic potential (MESP) on the iso-density surface ρ = 0.002 a.u. (Figure S1). The maxima and minima values of MESP are respectively found in regions of Br and N_{Py} atoms. As expected, the increase of the $MESP_{min}$ magnitude at N_{Py} is accompanied by that of the net negative charge $Q(N_{Py})$ (Table 2). Accordingly, the electrostatic ratio relative to the best acceptor $(MESP)_{acceptor}/(MESP)_{PyMe}$ follows the series of substituents CN < CF_3 < CO_2Me < Me (0.72, 0,79, 0,88 and 1,

respectively). As the donor moiety is the same in the four co-crystals, a roughly measure of the local electrostatic electrophilic•••nucleophilic interaction in adducts based on the MESP values obtained in monomers $\Delta(\text{MESP}) = (\text{MESP})_{max} - (\text{MESP})_{min}$ follows the same ranking along the series (73.2, 76.2, 80.1 and 85.3 kcal/mol, respectively). The structural distance Br•••N_{Py} in the adducts (Table 1), and therefore the reduction ratio (RR) of the Br•••N_{Py} halogen bonding interaction, decreases as the electrostatic descriptor of the electrophilic•••nucleophilic strength Δ(MESP) increases.

On the other hand, Table 2 also gathers the values of the negative laplacian of the electron density ($L = -\nabla^2\rho$) at the electrophilic charge depletion (CD) site of Br and at the nucleophilic charge concentration (CC) site of N_{Py} in donor and acceptor molecules. L_{CC} magnitudes are very close to each other, evolving inversely with respect to $MESP_{min}$ and $Q(N_{Py})$, whereas the quantities normalized per charge density unit $(L/\rho)_{CC}$ are almost equivalent with a maximum difference of only 1.3% between the extreme values. The descriptor $\Delta(L/\rho) = (L/\rho)_{CC} - (L/\rho)_{CD}$ has been used to measure the local electrostatic power of the electrophilic•••nucleophilic (CD•••CC) interaction.[11,17,20,21,22] Indeed, the more positive (negative) L/ρ value at CC (CD) site the greater the nucleophilic (electrophilic) power of the region, leading to a larger positive $\Delta(L/\rho)$ magnitude that measures the local electrostatic capability to assembly the complex. Accordingly, from the isolated molecules characterization, the local electrostatic electrophilic•••nucleophilic CD•••CC interaction is expected to be high and almost equivalent along the series of NBrSac•••PyX complexes ($77.8 < \Delta(L/\rho) < 78.0$ Å^{-2}), while $(L/\rho)_{CD}$ clearly dominates $(L/\rho)_{CC}$ in their contribution to the $\Delta(L/\rho)$ magnitude.

Polarizability in isolated molecules and NBrSac-adducts. The evolving behavior of the atomic polarizabilities from NBrSac and PyMe monomers to the NBrSac•••PyMe adduct is represented in Figure 2 (similar results are observed for the other adducts, see S.I. Figure S2). They have been calculated by fitting the linear dependency of the integrated atomic dipole moments obtained with AIMAll software[23] with respect to an external applied electric. This method is similar to another one found in the literature.[24] In isolated molecules, the most significant polarizabilities are found for the N_{Sac}, Br and N_{Py} atoms, indicating that their dipole moments follow the most significant variations among these of the other atoms under the influence of an external electric field. Further, as a consequence of the mutual influence in the adduct, their polarizabilities become even larger and more elongated along the N_{Sac}•••Br•••N_{Py} direction. This result points the significant capability of both halogen bonding interactions to polarize

their electron distributions under the effect of molecular environments, first upon the adduct formation, then once it is embedded in its crystalline environment. Hence, in order to get insight on the influence of polarizing environments on the electron distribution along the N_{Sac}•••Br•••N_{Py} halogen bonding motif, adducts have been subjected to the application of external electric fields, aimed to mimicking molecular and crystalline polarizing effects (see following sections). With this respect, it should be noted that electric polarizability has been used in this work as a driving force for the modification of atomic dipole moments, and therefore for electric field induced polarization on atomic electron distributions. Polarizability-polarizability interactions have not been investigated in this work, even if they also contribute to the full picture of electrostatic effects induced by polarizing environments. This further characterization, which merits additional investigations, is however out of the scope of this work.

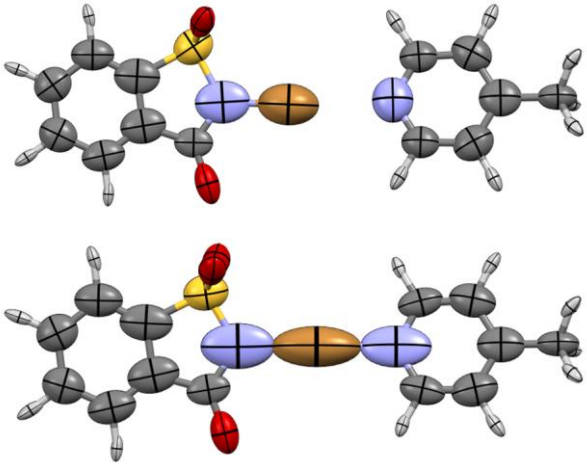

Figure 2. Atomic polarizabilities for (up) NBrSac and PyMe monomers and (down) NBrSac •••PyMe adduct in gas phase at experimental geometry.

Geometries of Br-adducts in gas-phase and crystal environments. Along the series of NBrSac adducts, theoretical (DFT periodic calculations) and experimental distances N_{Sac}•••Br/Br•••N_{Py} classify similarly, with theoretical values close to and systematically larger/shorter (0.04-0.07 Å) / (0.03-0.05 Å) than the experimental ones. Hence, in comparison with experimental results, and at actual the level of theory, the Br-atom is slightly shifted towards the acceptor with DFT periodic calculations. In all adducts except NBrSac •••PyMe, the differences are not significant enough to consider that the halogen atom has reached the middle position between donor and acceptor moieties.

The experimental geometries observed for NBrSac•••PyX adducts (X = CN, CF_3, CO_2Me, Me) indicate the progressive migration of the Br-atom towards PyX, the Br position becoming closer to the acceptor moiety along the X series CN > CF_3 > CO_2Me > Me (Table 1). Paralleling the larger/shorter N_{Sac}•••Br/Br•••N_{Py} distances, the topological (ρ) and energetic ($|V|/G$) properties calculated at the corresponding BCPs with adducts frozen at experimental geometries (Table 3) also indicate the concomitant weakening/strengthening of N_{Sac}•••Br/Br•••N_{Py} interactions along the same series, as previously observed in case of I-adducts.[11] Hence, as expected from the characterization of the MESP values at Br/N_{Py} atoms in monomers, larger electrophilic•••nucleophilic interactions lead to stronger Br•••N_{Py} assemblies in the adducts with the progressive migration of Br between donor and acceptor. Accordingly, the electronic effect of the substituent in the acceptor correlates with its assembly in the adduct, as previously observed in the case of hydrogen bond interactions that were characterized by the electrostatic potential and electric field magnitudes along the bonding direction.[25]

Figure 3 shows the position of the CPs of the L-function along the halogen bonding motif N_{Sac}•••Br•••N_{Py} of NBrSac•••PyMe (CPs are similarly placed in the other three adducts, Figure S3). Two (3,−3) CPs are within each nitrogen basin. Whereas the first one (closest to the nitrogen nucleus) corresponds to the nucleophilic CC site of the lone-pair and stands in a $L > 0$ region, the second one is placed at the border of the interatomic surface with the Br-atom and appears as a consequence of the bonding interaction (it does not exhibit in the monomer) while it stands in a $L < 0$ region. The saddle (3,−1) CP that shows between both (3,−3) CPs rises as a local 1D minimum along the direction linking the (3,−3) local maxima because of the continuity of the L-function in the space. In addition, actually belonging to the Br-atom, a pair of (3,−1) and (3,+1) CPs exhibit in both donor an acceptor sides. While the (3,−1) CP corresponds to the CD site ($L < 0$ region) in the valence-shell of the Br-atom, the (3,+1) CP stays within the closest inner shell of the atom ($L > 0$ region). Here, the (3,−1) CP appears between the (3,−3) and (3,+1) CPs as a consequence of the 1D local maxima of the two latter CPs along their linking direction and the continuity of the L-function. The $(L/\rho)_{CD}/(L/\rho)_{CC}$ values of Br/N_{Py} atoms in adducts at experimental geometries (Table 3) keep similar magnitudes than those observed in the corresponding individual molecules (Table 2), which show similar types and disposition of CPs. Hence, whereas at the CC site of N_{Py} the values are ~10% lower in adducts, they remain practically constant at the CD site of Br. Consequently, the electronic characterization obtained with individual molecules is able to approach a very good estimation of the $\Delta(L/\rho) = (L/\rho)_{CC} - (L/\rho)_{CD}$ magnitude observed in adducts (only a maximum difference of ~7% exhibits). On the

other hand, the $(L/\rho)_{CD}$ and $(L/\rho)_{CC}$ values corresponding respectively to Br and N_{Py} atoms do not change significantly from one complex to another (the maximum variation corresponds to ~5% at the CC site of N_{Py}). Consequently, along the series, the variation in the intensity of the local nucleophilic•••electrophilic interaction ($\Delta(L/\rho)/d^2_{CC\cdots CD}$) mainly depends on that of the distance $d_{CC\cdots CD}$. As expected, the $\Delta(L/\rho)/d^2_{CC\cdots CD}$ magnitude is significantly larger in the adducts than in those previously reported for intermolecular interactions,[22] whereas CC•••CD and internuclear directions are practically colinear (in both interactions of the halogen bonding motif and with all the adducts, Table 3).

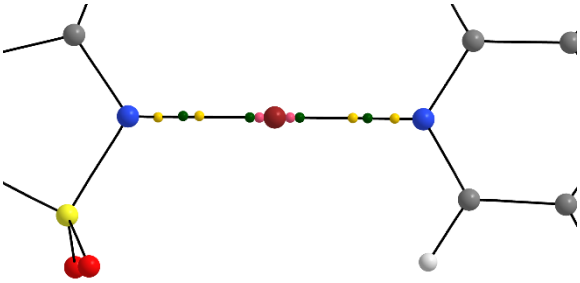

Figure 3. (3,−3) (yellow) and (3,−1) (green) and (3,+1) (pink) critical points of the *L*-function along the halogen bonding motif N_{Sac}•••Br•••N_{Py} of NSacBr•••PyMe at the experimental geometry. Whereas the CC sites correspond to the depicted (3,−3) CP closest to each N_{Sac} and N_{Py} nucleus, the CD sites correspond to the depicted (3,−1) CPs closest to the Br nucleus in donor and acceptor regions.

Table 3. Experimental and theoretical $d(N_{Sac}\cdots X)$ and $d(X\cdots N_{Py})$ internuclear distances (Å). Electron properties at (3,−1) BCPs of the $\rho(\mathbf{r})$-function calculated in gas-phase at frozen experimental geometries (including Br): electron density ρ (e/Å^3), Laplacian of the electron density $\nabla^2\rho$ (e/Å^5), local electron kinetic (*G*) and potential (*V*) energy densities (a.u.) and ratio $|V|/G$ (dimensionless). Electron properties at (3,−1)/(3,−3) CPs of the $L(\mathbf{r})$-function (atomic CD/CC sites) calculated in gas-phase at frozen experimental geometries (including Br): $d_{CC\cdots CD}$ distance (Å), negative Laplacian of the electron density $L = -\nabla^2\rho$ (e/Å^5) and its normalized quantity per charge density unit L/ρ (Å^{-2}), local electrostatic measure of the nucleophilic•••electrophilic interaction $\Delta(L/\rho) = (L/\rho)_{CC} - (L/\rho)_{CD}$ (Å^{-2}), its intensity $\Delta(L/\rho)/d^2_{CC\cdots CD}$ (Å^{-4}), and angle α (°) observed between CC•••CD and internuclear N•••Br directions. ε is the electric field applied to the adduct along the N_{Sac}•••N_{Py} direction to recover the experimental position of the Br-atom after its optimization in gas-phase.

NBrSac•••PyX adduct	**X = CN**	**X = CF_3**	**X = CO_2Me**	**X = Me**

Distances $d(N_{Sac}\bullet\bullet\bullet Br)$, $d(Br\bullet\bullet\bullet N_{Py})$:				
Experimental	1.967, 2.257	1.997, 2.204	2.004, 2.202	2.073, 2.098
Br-optimized	1.931, 2.293	1.934, 2.267	1.963, 2.243	1.962, 2.209
Periodic calculation	2.038, 2.204	2.069, 2.164	2.072, 2.173	2.114, 2.110
Gas-phase adduct frozen at experimental geometry:				
Topological and energetic properties of $\rho(\mathbf{r})$ at BCPs in $N_{Sac}\bullet\bullet\bullet Br$ and $Br\bullet\bullet\bullet N_{Py}$ regions:				
ρ	0.890, 0.484	0.837, 0.541	0.828, 0.546	0.715, 0.676
$\nabla^2\rho$	1.03, 2.99	1.31, 2.99	1.36, 2.93	1.91, 2.69
L/ρ	−1.16, −6.19	−1.57, −5.52	−1.65, −5.38	−2.66, −3.98
G	+0.0790, +0.0488	+0.0737, +0.0543	+0.0724, +0.0542	+0.0630, +0.0666
V	−0.1472, −0.0666	−0.1338, −0.0775	−0.1307, −0.0780	−0.1062, −0.1053
$\lvert V\rvert/G$	1.863, 1.365	1.815, 1.427	1.805, 1.439	1.686, 1.581
Topological properties at CC/CD sites of N/Br atoms in regions $N_{Sac}\bullet\bullet\bullet Br$ (first line) and $N_{Py}\bullet\bullet\bullet Br$ (second line):				
$d_{CC\cdots CD}$	1.1798	1.2191	1.2232	1.2945
	1.5087	1.4537	1.4517	1.3418
ρ_{CC}, ρ_{CD}	2.770, 28.094	2.855, 28.104	2.834, 28.109	2.887, 28.134
	3.630, 28.230	3.590, 28.215	3.568, 28.210	3.448, 28.178
L_{CC}, L_{CD}	+28.6, −1741.3	+28.8, −1741.0	+29.3, −1741.8	+30.9, −1741.3
	+52.1, −1748.5	+51.1, −1747.0	+50.5, −1746.9	+47.3, −1744.2
$(L/\rho)_{CC}, (L/\rho)_{CD}$	+10.3, −62.0	+10.1, −61.9	+10.3, −62.0	+10.7, −61.9
	+14.4, −61.9	+14.2, −61.9	+14.2, −61.9	+13.7, −61.9
$\Delta(L/\rho)$	72.3	72.0	72.3	72.6
	76.3	76.1	76.1	75.6
$\Delta(L/\rho)/d^2_{CC\bullet\bullet\bullet CD}$	51.9	48.5	48.3	43.3
	33.5	36.0	36.1	42.0
α	0.50	0.42	0.68	1.07
	0.24	0.17	0.33	0.14
Gas-phase adduct at experimental geometry with Br position optimized upon ε				
ε (GV/m)	1.28	2.05	1.28	2.96
Q (Br) (e)	+0.29	+0.29	+0.28	+0.29
Q (NBrSac/PyX) (e)	±0.18	±0.21	±0.22	±0.27
Q (NSac/Br–PyX) (e)	±0.48	±0.50	±0.50	±0.56

Mimicking molecular environment effects with electric field. Intermolecular environments further polarize and tune the assembly of the adducts. These additional effects can be mimicked by external electric fields ε.[26] Indeed, after relaxation of the Br-position in adducts with donor and acceptor moieties frozen at experimental geometries, the $N_{Sac}\bullet\bullet\bullet Br$ and $Br\bullet\bullet\bullet N_{Py}$ distances

differ from those found in crystals by $|\Delta d|$ = 0.03-0.11 Å (Table 3) as a consequence of the polarization induced by the molecular environment around the adducts. This electrostatic influence is measured by the magnitude of an external field that, applied along the adduct, permits to shift the Br-atom at the experimental position, retrieving the crystalline distances to donor and acceptor moieties. Accordingly, gas-phase calculations were carried out under the action of ε applied along the N_{Sac}•••N_{Py} direction, with magnitudes ranging $-40\times10^{-4} < \varepsilon < 100\times10^{-4}$ a.u. (1×10^{-2} a.u. = 5.1422082 GV/m). The electric field able to recover the experimental N_{Sac}•••Br and Br•••N_{Py} distances in the crystalline phase of the adducts is gathered in Table 3. It gives a measure of the overall electric field produced by the rest of the crystal that, added to the effect of the acceptor, is responsible for the experimental crystalline position of the Br-atom embedded in the adduct. The larger ε, the larger is the amplitude of donor and acceptor net charges, and therefore that of ionicity of moieties and crystals. This is measured by the integrated QTAIM net charges (Q) that were calculated for the fragments, with Br belonging to either donor or acceptor molecule. In both cases, the picoline adduct NBrSac•••PyMe exhibits the largest amplitude of net charges among the four adducts, result that is brought close to its more important Br-atom migration within the adduct.

On the other hand, it is noteworthy the almost constant net charge of the Br-atom (Q(Br) ≅ +0.29-0.30 e) from one to another adduct (Table 3), despite their different intra- and intermolecular influences. A similar result was previously observed with other donor-acceptor I-adducts, where Q(I) ≅ +0.42-0.45 e.[11] The structural information obtained for the four adducts shows that the Br-atom position is closer to the donor in all of them. Although this feature seems to indicate that, for any substituent (X = CN, CF_3, CO_2Me, Me), the NBrSac/PyX charge partition should be considered rather than $[NSac]^-/[Br–PyX]^+$ at the crystalline geometry, this can be only fully assessed with the analysis of the electronic properties in both N_{Sac}•••Br and Br•••N_{Py} regions.

Migrating the Br position in Br-adducts upon the action of ε. For each adduct, the bonding distance, net charge Q(Br), topological and energetic properties at BCP, as well as the corresponding delocalization index (*DI*),[27] have been calculated for both N_{Sac}•••Br and Br•••N_{Py} interactions (Tables S1 to S4) with each applied electric field ($-40\times10^{-4} < \varepsilon < 100\times10^{-4}$ a.u.). Results concerning the NBrSac•••PyMe adduct are shown in Figure 4 (for the three other adducts see Figures S4 to S6). Upon the application of ε (Figure 4a), the Br-atom shifts its position within the adduct. Thus, in Figure 4b, the N_{Sac}•••Br bond distance increases as a

function of the amplitude $\varepsilon > 0$ of the applied external electric field. Within the range of applied fields, a polynomial function of third-order fits very well the hold dataset (R^2 = 0.9999), whereas for larger magnitudes a linear dependence appears. At ε = 0, the N_{Sac}•••Br distance (1.962 Å) is shorter than the experimental one (2.073 Å). The application of a magnitude of ε = 2.96 GV m^{-1} is needed to retrieve the experimental geometry, measuring the significant effect of the crystalline environment in polarizing the actual charge distribution within the halogen-bonded complex. This value falls well in the range of values felt by molecules in crystals (∼1−20 GV m^{-1}),[28,29,30] and is close to those observed in proteins and enzymes (∼5 GV m^{-1}).[31,32] The elongation of the N_{Sac}•••Br distance with $\varepsilon > 0$ parallels in the same measure the shortening of Br•••N_{Py}, because the N_{Sac}•••Br•••N_{Py} motif is almost linear (177.4°). Hence, translating the variation of distances in terms of effective electric fields ($\varepsilon > 0$) applied from ε = 0, the increase/decrease of N_{Sac}•••Br/Br•••N_{Py} distances is $|\Delta d|$ = 0.116 Å (d(N_{Sac}•••Br) = 2.078 Å, d(Br•••N_{Py}) = 2.093 Å) for an applied field of ε = 60 × 10^{-4} a.u. (3.09 GV m^{-1}), which is close to the magnitude needed to retrieve the experimental crystalline geometry of the NBrSac•••PyMe adduct (d(N_{Sac}•••Br) = 2.073 Å and d(Br•••N_{Py}) = 2.098 Å, for ε = 57.7 × 10^{-4} a.u. = 2.96 GV m^{-1}). From ε = 0, and for the same applied field and resulting $|\Delta d|$, the observed variations of ρ and $|V|/G$ at BCPs of N_{Sac}•••Br/Br•••N_{Py} interactions are respectively (in percentage): −22/+30 % and −12/+15 %. Accordingly, the variation of the Br•••N_{Py} strengthening is found slightly larger than the N_{Sac}•••Br weakening upon the applied ε. This trend, which is similar for other $\varepsilon > 0$ magnitudes, points the unbalanced effect of the polarizing crystalline environment at donor and acceptor sides in the assembly of the adduct.

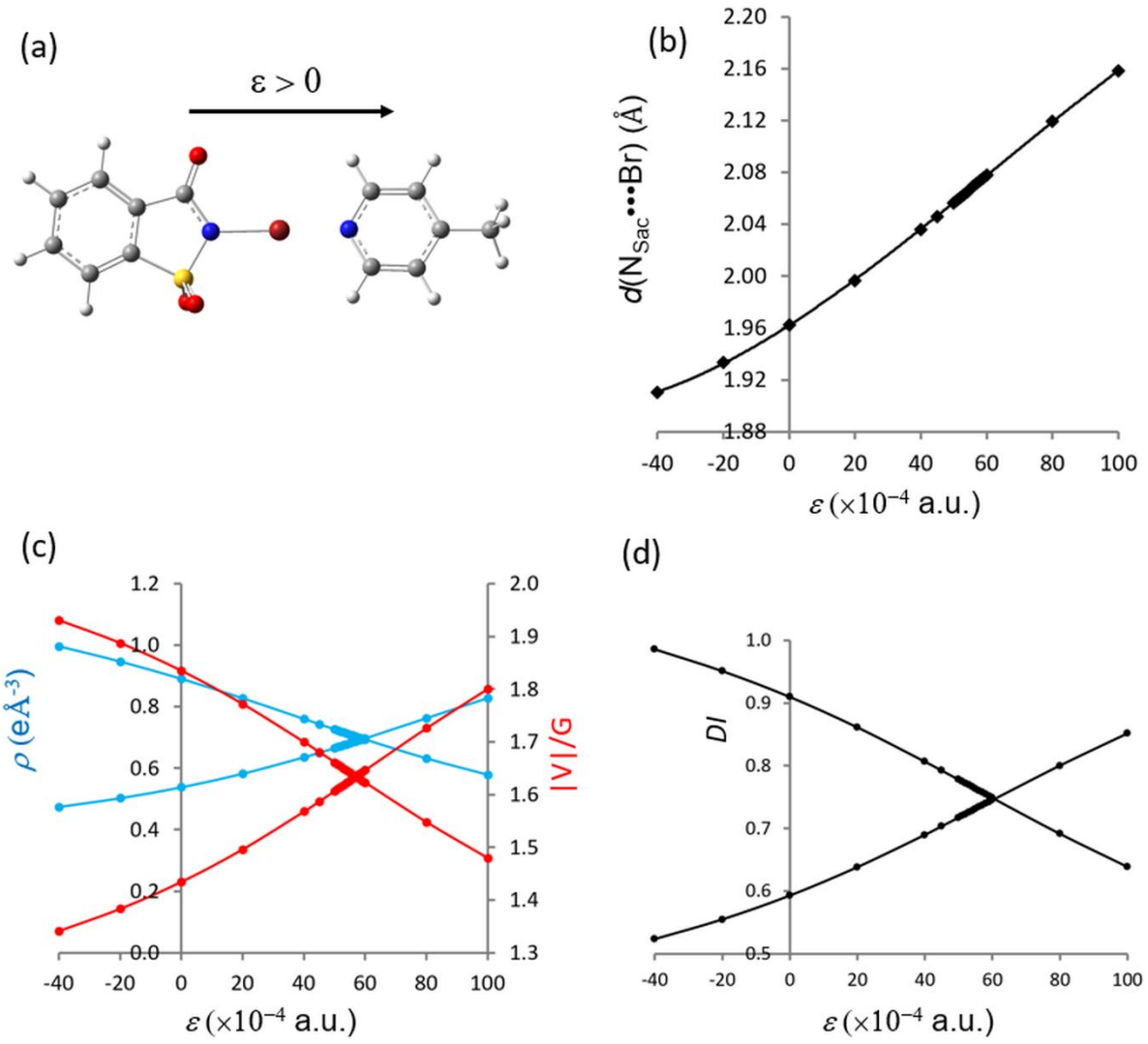

Figure 4. (a) NBrSac•••PyMe adduct frozen at the experimental geometry except for the Br-atom position, which has been optimized upon the application of an external electric field ranging $-40\times10^{-4} < \varepsilon < 100\times10^{-4}$ (a.u.), (b) $d(N_{Sac}\bullet\bullet\bullet Br)$ (Å) *vs* ε (a.u.), the depicted fitting function is $d(N_{Sac}\bullet\bullet\bullet Br) = -4\cdot10^{-8}\cdot\varepsilon^3 + 7\cdot10^{-6}\cdot\varepsilon^2 + 1.6\cdot10^{-3}\cdot\varepsilon + 1.9621$ (correlation factor R^2 = 0.9999). The corresponding ε *vs* $d(N_{Sac}\bullet\bullet\bullet Br)$ curve leads to the fitting function $\varepsilon = (5277.7)\times d^3 - (32807.5)\times d^2 + (68440.2)\times d - 47849.9$ (correlation factor R^2 = 0.99997), (c) ρ (blue curves and left scale in eÅ^{-3}) and $|V|/G$ (red curves and right scale dimensionless) at $N_{Sac}\bullet\bullet\bullet Br/Br\bullet\bullet\bullet N_{Py}$ BCPs (decreasing/increasing curves), and (d) delocalization index (*DI*) *vs* ε for $N_{Sac}\bullet\bullet\bullet Br/Br\bullet\bullet\bullet N_{Py}$ interactions (decreasing/increasing curves). In (c) and (d), depicted curves are plotted for guiding eyes.

From Figure 4b, the polarizing effect induced by ε on the electron distribution drives the position of bromine between donor and acceptor moieties. From geometric considerations only, it is not however possible to conclude that the exact middle position within the adduct corresponds to the formal limit of the Br-transfer between molecules, because nitrogen atoms N_{Sac} and N_{Py} are not electronically equivalent. With this aim, we have calculated ρ and $|V|/G$ at both BCPs (Figure 4c), and *DI* (Figure 4d), for N_{Sac}•••Br and Br•••N_{Py} interactions. Whereas ρ and $|V|/G$ at BCP inform about the strength of the interaction by means of the accumulated charge density and the covalence degree of the interaction ($1 < |V|/G < 2$),[33] *DI* is a measure of the bond order.[27] Thus, from electronic considerations, it is expected that the strongest interaction would show up with larger magnitudes of these properties. Following the shift of the Br-position with $\varepsilon > 0$, all of them decrease/increase in N_{Sac}•••Br/Br•••N_{Py} regions. For each quantity, the intersection of the variations observed for N_{Sac}•••Br and Br•••N_{Py} interactions marks the electric field that is able to balance the strength at donor and acceptor sides, and therefore the formal geometry at which the Br-atom position is in the limit situation of the transfer. Table 4 gathers the electric fields ε corresponding to the intersections found for ρ, $|V|/G$ and *DI* curves, as well as the distances calculated upon the action of ε (from the fitting curves $d(N_{Sac}\bullet\bullet\bullet Br) = f(\varepsilon)$ of Figure 4b and Figures S4b to S6b, and the corresponding distances $d(Br\bullet\bullet\bullet N_{Py}) \approx d_{exp}(N_{Sac}\bullet\bullet\bullet N_{Py}) - d(N_{Sac}\bullet\bullet\bullet Br)$ taking into account that the geometry N_{Sac}•••Br•••N_{Py} is almost linear). Whereas it should be noted the approximation of the procedure (except the Br-atom, the rest of the adduct is frozen to keep the experimental geometry, in particular the N_{Sac}•••N_{Py} distance, throughout the range of applied electric fields), it permits to get insight from several trends. Thus, for all the adducts, the maximum and minimum values of ε along the three properties are very similar within a range of only $\approx 4 \times 10^{-4}$ a.u. (0.2 GV m^{-1}), which translates to $|d| < 0.007$ Å in terms of distances. This feature indicates the intrinsic consistency of ρ, $|V|/G$ and *DI* in pointing the limiting geometry of the atomic transfer within a range of 0.007 Å, even if it is systematically observed that first $|V|/G$, then ρ and *DI* are balanced along the shift of the Br-atom. On the other hand, following the experimental geometries and the electronic properties of individual molecules and adducts at experimental geometries, the decreasing value of ε that is needed for reaching the geometry of the Br-transfer among the adducts (Table 4) also ranks the increasing acceptor strength that shows along the series PyCN < $PyCF_3$ < $PyCO_2Me$ < PyMe. The differences in the power of the substituents to pull the Br-atom can be measured in terms of the relative differences of ε to balance the strength of the Br interactions at donor and acceptor sides. Hence, with respect to PyMe, the derivatives

$PyCO_2Me$, $PyCF_3$ and PyCN weaken respectively in terms of a less polarizing electric field of approximately 9, 23 and 26 $\times 10^{-4}$ a.u. (*i.e.*, ~ 0.45, 1.15 and 1.3 GV m^{-1}). Accordingly, the effect of substituents along the family can be estimated within a range of ~ 1.3 GV m^{-1}.

Table 4. Magnitude of the electric field ε ($\times 10^{-4}$ a.u.) applied to the adduct to balance the electron property (ρ, |V|/G or *DI*) at N_{Sac}•••Br and Br•••N_{Py} interactions in each adduct NBrSac •••PyX (X = CN, CF_3, CO_2Me, Me). For each electron property, the expected $d(N_{Sac}$•••X) and $d(X$•••$N_{Py})$ distances for the limit of the Br-transfer are calculated by using the fitting functions $d(N_{Sac}$•••X) = f(ε) (see Figures 4 and S3-S5) and $d(X$•••$N_{Py}) \approx d(N_{Sac}$•••$N_{Py})_{exp} - d(N_{Sac}$•••X). For comparison, geometries obtained from experimental data and periodic calculations are also given. ε magnitudes are given within intervals of 0.5×10^{-4} a.u. (≈ 0.025 GV m^{-1}), which correspond approximately to distance variations < 0.001 Å.

NBrSac•••PyX	**X = CN**	**X = $PyCF_3$**	**X = CO_2Me**	**X = Me**
ε at intersection				
ε(|V|/G)	83	80	66	57
$\varepsilon(\rho)$	85.5	82.5	67.5	59.5
$\varepsilon(DI)$	87	84.5	70	60.5
$d(N_{Sac}$•••Br) and $d(Br$•••$N_{Py})$ (Å) by using:				
$\varepsilon(\|V\|/G)$	2.094, 2.130	2.087, 2.114	2.094, 2.077	2.069, 2.102
$\varepsilon(\rho)$	2.100, 2.124	2.092, 2.109	2.098, 2.073	2.074, 2.097
$\varepsilon(\|DI)$	2.104, 2.120	2.097, 2.104	2.103, 2.068	2.076, 2.095
Experimental data	1.967, 2.257	1.997, 2.204	2.004, 2.202	2.073, 2.098
Periodic calculation	2.038, 2.204	2.069, 2.164	2.072, 2.173	2.114, 2.110

While keeping in mind the approximation previously indicated, NBrSac•••PyX (X = CN, CF_3 and CO_2Me) adducts at experimental geometries are relatively far from the limit of the Br-transfer (Table 4). This does not seem however the case of NBrSac•••PyMe, for which the experimental geometries are within the very short range of formal distances (pointed by the

electronic properties) where the Br interactions with donor and acceptor are balanced, indicating that the Br-atom is in the limit of the transfer (Table 4). Nevertheless, for all the adducts, it should be noted that, at any investigated geometry, a significant covalence degree ($1 < |V|/G < 2$) shows at both donor and acceptor sides, whereas the delocalization index $DI(N_{Sac}|N_{Py})$ is non-negligible (for instance, at experimental geometries, it accounts 0.085, 0.090, 0.092 and 0.099 for adducts with PyCN, $PyCF_3$, $PyCO_2Me$ and PyMe acceptors, while the reference cases of formamide and $[F{-}H{-}F]^-$ exhibit respectively $DI(N|O) = 0.30$ and $DI(F|F) = 0.22$). Consequently, adducts should be considered as a unique molecular entity rather than two, assembled with a non-negligible contribution of three-center four-electrons interaction.

In this context, the transfer of the Br-atom, which accompanies a closer position of the Br-atom to the acceptor, helped by the weak N_{Sac}•••Br bond and the strong Br•••N_{Py} interaction and pulled by the electric field, increases significantly the dipole moment of the adducts (Figure 5). Figures 2 and S2 point the atoms of the N_{Sac}•••Br•••N_{Py} motif as the main contributors to the dipole moment of the adducts. In the range $0 < \varepsilon < 100$ ($\times 10^{-4}$ a.u.), the increasing behavior of the dipole moment is linear for all the adducts (blue data), rising by a difference of ~ 20, 14, 15 and 23 Debye with respect to the reference geometry at $\varepsilon = 0$ for adducts with PyCN, $PyCF_3$, $PyCO_2Me$ and PyMe acceptors, respectively. Even with the actual approximation (all the atoms except Br are frozen at the experimental geometry in the adducts), this is a quite significant behavior. Indeed, it is expected that the perturbation induced by the polarizing field ε affects less the relative position of the negative moieties NSac and PyX (which polarize their electron distributions in the same way) than that of the positive Br-atom among them (Tables S1 to S4) pulled towards PyX for all the studied derivatives with $\varepsilon > 0$. For comparison with another external perturbation, the recent experimental study of the NISac•••Py adduct under pressure[34] shows a quite small shortening of the N_{Sac}•••N_{Py} distance upon crystal compression ($4.40 < d_{NSac\cdots NPy} < 4.53$ Å, leading to $\Delta d \sim 2.9$ % for $\Delta P \sim 4.5$ GPa) that is accompanied by the shift of the I-atom towards N_{Py}. Upon this external constraint, the halogen atom shifts beyond the middle position within the adduct, as shown by the variation of the normalized bonding distance (N_{Sac}•••I)/(N_{Sac}•••N_{Py}), which becomes greater than 0.5 along the almost linear N_{Sac}•••I•••N_{Py} halogen bonding motif.

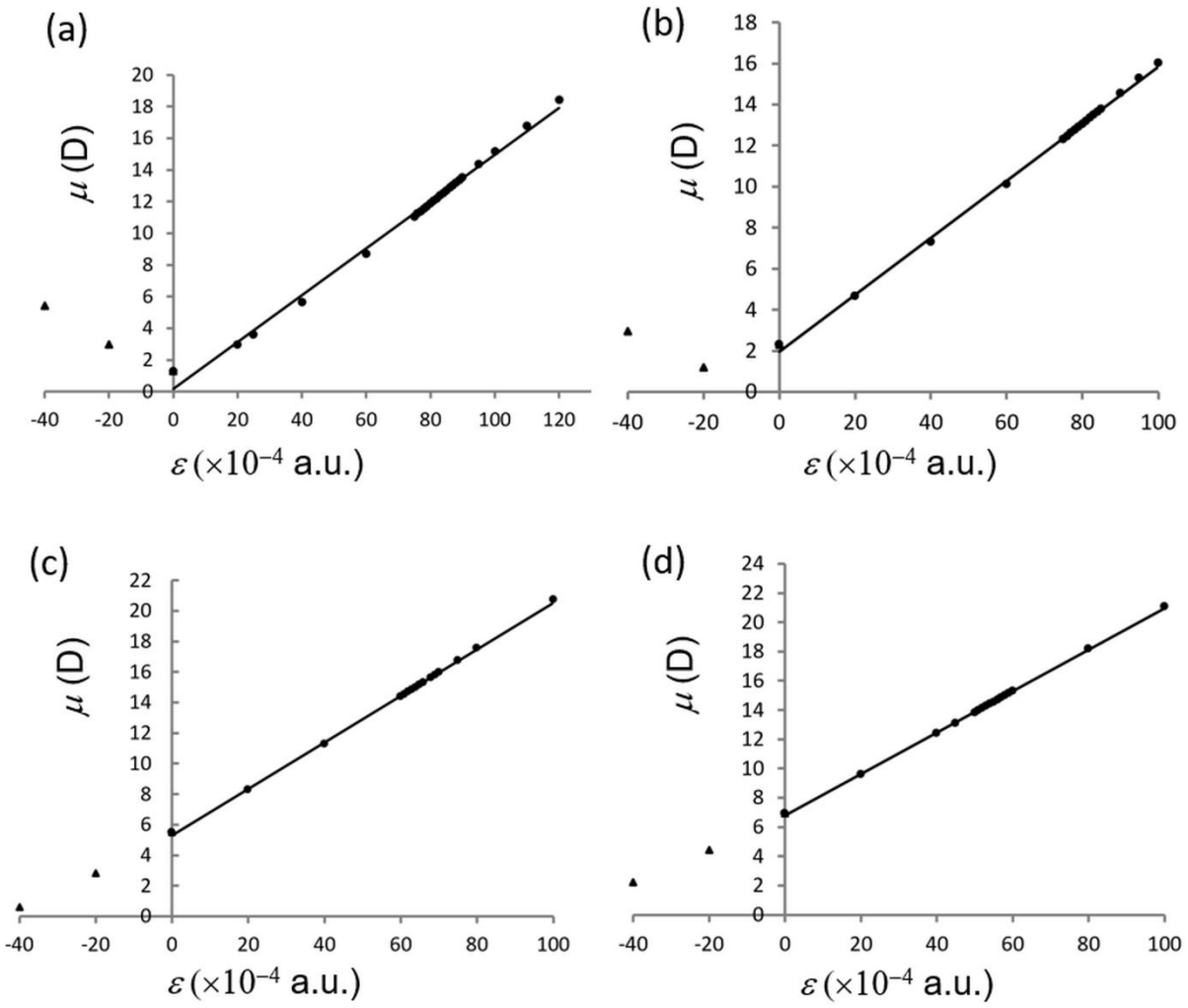

Figure 5. Dipole moment μ (Debye) of adducts NBrSac•••PyX as a function of ε. The fitting curves involve $\varepsilon > 0$ data only (black filled circles): (a) X = CN, fitting function: $\mu = 0.1493 \times \varepsilon + 0.0849$ ($R^2 = 0.9944$), (b) X = CF_3, fitting function: $\mu = 0.1386 \times \varepsilon + 1.9739$ ($R^2 = 0.9988$), (c) X = CO_2Me, fitting function: $\mu = 0.1524 \times \varepsilon + 5.2916$ ($R^2 = 0.9994$), (d) X = Me, fitting function: $\mu = 0.1426 \times \varepsilon + 6.7425$ ($R^2 = 0.9998$).

Finally, to completely asses the effect of polarizing environments on the halogen bonding interactions at donor and acceptor sides, electronic properties have been also characterized at local electrophilic (CD) and nucleophilic (CC) sites in the valence-shell of Br and N_{Sac}/N_{Py} atoms. Types and alternance of CPs along the N_{Sac}•••Br•••N_{Py} motif are the same as those observed in the adducts frozen at experimental geometries (Figures 3 and S3). Table 5 summarizes the magnitudes observed at CC/CD sites for the extreme fields $\varepsilon = 0$ and $\varepsilon = 100 \times 10^{-4}$ a.u. (intermediate magnitudes with monotonic behavior show along the range $0 < \varepsilon < 100 \times 10^{-4}$ a.u.). For the four adducts, the electronic properties at donor and acceptor sides, as

well as the relative orientation of CC•••CD and internuclear directions (practically colinear in all cases), do not exhibit significant variations with ε. Only $\Delta(L/\rho)/d^2_{CC\cdots CD}$ magnitudes are affected as a consequence of the variation of the $d_{CC\cdots CD}$ distances, which follow the Br-atom shift with ε. In addition, all the investigated properties associated to CC/CD sites are very similar to those obtained with the systems extracted from the crystal structures frozen at experimental geometries. Hence, these results point noteworthily three main features: (i) local electrophilic•••nucleophilic interactions are orienting bonding interactions by facing to each other CC and CD sites along internuclear directions, (ii) the characterized properties are intrinsically related to the electronic structure of the atom in the molecule (and therefore closely similar to those observed in the corresponding individual molecules), and (iii) they are consequently subjected to little external influence from crystalline polarizing environments.

Table 5. Topological properties upon the application of electric fields ε and calculated at the (3,−3) and (3,−1) critical points of $L(\mathbf{r})$ that are associated to nucleophilic charge concentration (CC) and electrophilic charge depletion (CD) sites in the valence-shell of N_{Sac}/N_{Py} and Br atoms. Only results obtained for the extreme investigated fields ε = 0 and 100 ($\times 10^{-4}$ a.u.) are gathered (intermediate fields lead to properties with intermediate monotonic values). Depicted properties have the same definitions and units than in Table 3. First and second lines correspond to values in donor N_{Sac}•••Br and acceptor Br•••N_{Py} regions.

Adduct	ε	$d_{CC\cdots CD}$	$(L/\rho)_{CC}$, $(L/\rho)_{CD}$	$\Delta(L/\rho)$	$\Delta(L/\rho)/d^2_{CC\cdots CD}$	α
NBrSac•••PyCN	0	1.1420	10.4, −62.0	72.4	55.5	0.14
		1.5461	14.5, −62.0	76.4	32.0	0.51
	100	1.3698	11.5, −61.8	73.3	39.1	0.51
		1.3180	12.8, −61.9	74.7	43.0	0.56
NBrSac•••$PyCF_3$	0	1.1505	10.4, −62.0	72.4	54.7	2.06
		1.5192	14.4, −61.9	76.4	33.1	0.06
	100	1.3714	11.5, −61.8	73.4	39.0	3.09
		1.3040	12.8, −61.9	74.8	44.0	0.19
NBrSac•••$PyCO_2Me$	0	1.1846	10.2, −62.0	72.2	51.5	0.84
		1.4952	14.3, −61.9	76.2	34.1	0.24
	100	1.3987	11.6, −61.9	73.5	37.6	0.81
		1.2711	12.6, −62.0	74.6	46.1	0.37
NBrSac•••PyMe	0	1.1785	10.7, −62.0	72.6	52.3	0.53
		1.4569	14.1, −61.9	76.0	35.8	0.18
	100	1.3920	11.8, −61.8	73.7	38.0	0.76
		1.2421	12.5, −62.0	74.5	48.3	0.13

Conclusions

The good halogen bond donor NBrSac has been co-crystallized with four good halogen bond acceptors (PyCN, $PyCF_3$, $PyCO_2Me$ and PyMe). Their crystal structures have been determined and permitted to observe the formation of adducts with a significant weakening of the N_{Sac}•••Br bonding interaction with respect to the isolated NBrSac XB donor, as well as the formation of a strong Br•••N_{Py} interaction. The molecular electrostatic potential (MESP) calculated with the different pyridines indicates a larger negative magnitude at the N_{Py} nitrogen along the series of acceptors PyCN < $PyCF_3$ < $PyCO_2Me$ < PyMe, correlating with shorter Br•••N_{Py} distances along the same series in their adducts at crystalline geometries.

The atomic polarizabilities calculated in the individual donor and acceptor molecules clearly show that the dipole moments of the N_{Sac}, Br and N_{Py} atoms are the mainly affected by an external electric field. Then, going from individual molecules to adducts, the influence of the additional molecular environment still amplifies their polarizabilities with respect to the rest of surrounding atoms. As the increase of the atomic dipole moment is related to a larger separation of positive and negative charges in the atom, this effect points the significant propensity of their electron distributions to be affected by polarizing effects of molecular environments.

The topological properties at the N_{Sac}•••Br•••N_{Py} bond critical points (BCPs) of the adducts frozen at experimental geometries, point the increasing strength of the studied acceptors along the series PyCN < $PyCF_3$ < $PyCO_2Me$ < PyMe, correlating with the structural distances of their halogen bonding motifs and the larger negative MESP values in their monomers.

In order to explore the effect of polarizing environments on the halogen bonding regions N_{Sac}•••Br•••N_{Py}, an external electric field has been applied ($-40\times10^{-4} < \varepsilon < 100\times10^{-4}$ a.u.) to adducts extracted from experimental geometries with all atoms frozen except Br, which has been optimized as a function of ε. At $\varepsilon = 0$, all the adducts show the Br-atom coming back to the donor, pointing the effect of the crystalline environment in the experimental position of the halogen atom within the adduct. This effect, translated in terms of an effective electric field, ranges from 1.28 to 2.96 GV m^{-1} for the four adducts. It gives a measure of the overall electric field produced by the rest of the crystal in the halogen bonding motif of the adducts. The Br-atom approaches the acceptor with the increase of ε. An excellent polynomial fitting function

of 3rd-order permits to derive the straightforward relationship of the N_{Sac}•••Br distance with ε (R^2 factors are as good as 0.9999 for the four adducts), and inversely.

The topological properties ρ and $|V|/G$ at both BCPs, as well as the values of the delocalization index $DI(N_{Sac}|Br)$ and $DI(Br|N_{Py})$, have permitted to follow the weakening/strengthening of the N_{Sac}•••Br/Br•••N_{Py} interactions with the shift of the Br-atom with $\varepsilon > 0$. For each electronic property, the applied field ε at which the decreasing/increasing tendencies observed in donor/acceptor regions cross to each other permits to derive the border geometry in the transfer between donor and acceptor moieties, because the strength of the interactions is formally equivalent at both sides of the halogen atom. For each adduct, the magnitude of that field is very similar from one electron property to other. The range of fields balancing both N_{Sac}•••Br/Br•••N_{Py} interactions for the three properties ($\Delta\varepsilon \approx 4 \times 10^{-4}$ a.u. = 0.2 GV m^{-1}) translates into to a range of distances $|\Delta d| < 0.007$ Å. The differences in the power of the substituents to pull the Br-atom towards the acceptor can be measured in terms of the relative differences of ε to balance the strength of the Br interactions at donor and acceptor sides. Thus, the comparison of the fields observed for the four adducts indicate again that the increasing acceptor strength follows the series PyCN < $PyCF_3$ < $PyCO_2Me$ < PyMe, their effect along the family ranging by $\Delta\varepsilon \approx 26 \times 10^{-4}$ a.u. = 1.34 GV m^{-1}. Among the four adducts at experimental geometries, only NBrSac•••PyMe reaches the region of distances where the analyzed electronic properties balance at donor and acceptor sides.

At any investigated geometry (*i.e.*, within the full range of applied fields), the adducts exhibit significant covalence degree ($1 < |V|/G < 2$) and *DI* magnitudes at both donor and acceptor sides. These features lead to the conclusion that the adducts should be considered as a unique molecular entity rather than two. In addition, at experimental geometries, $DI(N_{Sac}|N_{Py})$ accounts 0.085, 0.090, 0.092 and 0.099 in the adducts with PyCN, $PyCF_3$, $PyCO_2Me$ and PyMe acceptors, pointing assemblies with a small but non-negligible contribution of a three-center four-electrons interaction.

With this family of donor-acceptor adducts, and in spite of the approximation used in calculations (donor and acceptor moieties are frozen at experimental geometries, while the Br-atom position is optimized), it has been revealed that the Br-atom can shift significantly towards acceptors with the application of ε, while the Br position is fully correlated with the dipole moment of adduct. The variation of the latter ranges from one to two tenths of Debye's within the range of investigated fields from $\varepsilon = 0$. This is a very interesting trend that merits further investigations. Indeed, under an external constrain such as an electric field, pressure or

temperature, the modification of the halogen position and therefore of the dipole moment of the molecular unit formed after the assembly of the adducts could be used in applications based on the tuning of molecular dipole moments.

Finally, the influence of polarizing environments does not seem to play a significant role neither in the position nor in the electron properties of the electrophilic (CD)/nucleophilic (CC) sites found in the valence-shell of Br/N atoms. This trend is brought close to their own intrinsic character, which is mainly associated to the electron distribution of the atom within its molecule. Consequently, the characteristic magnitudes derived for individual molecules (monomers or isolated molecules at crystalline geometries) can be used (with a good degree of approximation) to understand molecular orientation and assembly in crystalline environments, as CC and CD sites are facing each other along internuclear directions of atoms that are in bonding interaction.

Experimental Section

NBrSac and the different pyridines were commercially available and used as received. 300 MHz (^{1}H) NMR spectra were recorded on Bruker Avance 300 spectrometer at room temperature using perdeuterated solvents as internal standards. Elemental analyses were performed by the Service Central d'Analyses du CNRS, Vernaison, France.

Syntheses and Crystal Growth.

NBrSac and 4-cyanopyridine. NBrSac (15 mg, 5.72×10^{-5} mol) was dissolved in 1,2-dichloroethane (2 mL) and 4-cyanopyridine (12 mg, 11.44×10^{-5} mol) was added. The solution was filtered to remove non-dissolved particles and poured in a Durham tube. Crystals were obtained by vapor diffusion method with hexane. The sample was left to 2°C during 8 days in the dark. White crystals were obtained. M. p. 151–152°C. ^{1}H NMR (300 MHz, Acetonitrile-d_3) δ 8.88–8.77 (m, 2H, Ar(CNPy)), 8.14–7.86 (m, 4H, Ar (NBrSac)), 7.78–7.68 (m, 2H, Ar (CNPy)). Elem. Anal. Calcd. for $C_{13}H_8BrN_3O_3S$: C 42.62, H 2.20, N 11.48%. Found C 42.44, H 2.17, N 11.25 %.

NBrSac and 4-trifluoromethylpyridine. NBrSac (15 mg, 5.72×10^{-5} mol) was dissolved in dichloromethane (2 mL) and 4-trifluoromethylpyridine (17 mg, 14 μL, 11.44×10^{-5} mol) was added. The solution was filtered to remove non-dissolved particles and poured in a Durham tube. Crystals were obtained by vapor diffusion method with hexane. The sample was left at

2°C during 8 days in the dark. White crystals were obtained. M. p. 96°C. ^{1}H NMR (300 MHz, Acetonitrile-d^{3}) δ 8.86 (d, J = 5.2 Hz, 2H, Ar (Py-CF_3)), 8.18–7.82 (m, 4H, Ar NBrSac), 7.78–7.59 (m, 2H, Ar (Py-CF_3)). El. Anal. Calcd. for $C_{13}H_8BrF_3N_2O_3S$ (409.178 g/mol): C 38.16, H 1.97, N 6.85% Found: C 37.07, H 1.86, N 6.52 %.

NBrSac and 4-methylisonicotinate. NBrSac (15 mg, 5.72 × 10^{-5} mol) was dissolved in 1,2-dicloroethane (2 mL) and 4-methylisonicotinate (15 μL, 11.44 ×10^{-5} mol) was added. The solution was filtered to remove non-dissolved particles and poured in a Durham tube. Crystals were made by vapor diffusion method with hexane left to 2°C during 8 days in the dark. White needle-shaped crystals were obtained. M. p. 158–159°C. ^{1}H NMR (300 MHz, DMSO-d_6) δ 9.02–8.88 (m, 2H, Ar (MIC)), 8.38–7.76 (m, 6H, Ar (MIC) + Ar (NBrSac)), 3.93 (s, 3H, Me). Elem. Anal. Calcd. for $C_{14}H_{11}BrN_2O_5S$: C, 42.12; H, 2.78; N, 7.02 %. Found C 42.16, H 2.71, N 6.89 %.

X-ray Crystallography. X-ray crystal structure collections were performed on an D8 Venture Bruker-AXS diffractometer equipped with a CCD camera and a graphite-monochromated Mo–Kα radiation source (λ = 0.71073 Å) at 150 K. Details of the structural analyses are summarized in Table 6. Absorption corrections were performed with SADABS. Structures were solved by direct methods using the *SIR97* program,[35] and then refined with full-matrix least-square methods based on F^2 (*SHELXL-97*)[36] with the aid of the *WINGX* program.[37] All non-hydrogen atoms were refined with anisotropic atomic displacement parameters. H atoms were finally included in their calculated positions. CCDC 2247485-2247487 contain X-ray crystallographic files in CIF format for this paper. These data can be obtained free of charge via www.ccdc.cam.ac.uk/data_request/cif, or by emailing data_request@ccdc.cam.ac.uk, or by contacting The Cambridge Crystallographic Data Centre, 12 Union Road, Cambridge CB2 1EZ, UK; fax: + 44 1223 336033

Table 6. Crystallographic data

	NBrSac•PyCO$_2$Me	NBrSac•PyCF$_3$	NBrSac•PyCN
CCDC	2247486	2247487	2247485
Formula	$C_{14}H_{11}BrN_2O_5S$	$C_{13}H_8BrF_3N_2O_3S$	$C_{13}H_8BrN_3O_3S$
FW (g.mol^{-1})	399.22	409.18	366.19
System	orthorhombic	monoclinic	monoclinic
Space group	Pbca	P2$_1$/n	P2$_1$/c
a (Å)	7.8267(4)	6.9218(2)	7.1589(2)
b (Å)	16.1414(9)	15.1624(4)	13.6851(4)
c (Å)	24.0082(14)	14.4948(3)	14.7414(4)
α (deg)	90.00	90.00	90.00
β (deg)	90.00	100.9340(10)	102.0370(10)
γ (deg)	90.00	90.00	90.00
V (Å^3)	3033.0(3)	1493.63(7)	1412.46(7)
T (K)	150(2)	150(2)	150(2)
Z	8	4	4
D_{calc} (g.cm^{-1})	1.749	1.82	1.722
μ (mm^{-1})	2.875	2.94	3.071
Total refls	62039	6560	5926
Abs corr	multi-scan	multi-scan	multi-scan
T_{min}, T_{max}	0.691, 0.842	0.735, 0.943	0.308, 0.509
θ_{max} (°)	27.507	30.539	27.488
Uniq refls	3483	4532	3122
R_{int}	0.051	0.0221	0.0118
Uniq refls (I > 2σ(I))	3063	3893	2956
R_1	0.0213	0.0415	0.0219
wR_2 (all data)	0.0541	0.1117	0.0561
GOF	1.046	1.052	1.102
Res. dens. (e Å^{-3})	–0.327, 0.06	–1.065, 0.11	–0.513, 0.066

Theoretical calculations and methods. Gas-phase calculations (Gaussian09)[38] of monomers (donor and acceptors) at optimized geometries were carried out at the PBEPBE-D2 aug-cc-pVTZ level of theory. The electron properties focused in the analyzed monomers are: (i) the integrated charge (*Q*) of Br and N_{Py} in their atomic basins,[39] (ii) the molecular electrostatic

potential (MESP) on the iso-density surface ρ = 0.002 a.u., (iii) the values of the negative laplacian $L(\mathbf{r}) = -\nabla^2\rho(\mathbf{r})$ and (iv) the electron density $\rho(\mathbf{r})$ at relevant charge depletion (CD) and charge concentration (CC) sites of Br and N_{py} atoms in the external parts of donor and acceptor monomers (Table 2). The topological critical points of the $L(\mathbf{r})$ function[40,41,42] can be used to determine the electrophilic/nucleophilic (CD/CC) sites in the valence-shell of atoms. Thus, for either light or heavy atoms, lone-pairs and their corresponding nucleophilic CC sites are determined by (3,−3) CPs of L, whereas electrophilic regions (CD sites) can be characterized by either (3,−1) CPs (found with heavy atoms, like I, Br or Se) or the more common (3,+1) CPs found with lighter elements having a less number of electron-shells.[11,17,20,21,22] Accordingly, for monomers and adducts, the electrophilic (CD)/nucleophilic (CC) sites of Br/N atoms are characterized by (3,−1)/(3,−3) CPs of the $L(\mathbf{r})$ function. The electronic properties at the topological critical points (CPs) of the $L(\mathbf{r})$ function have been calculated with the AIMAll software.[23]

Periodic DFT calculations at the DFT level of theory (PBE functional; Dispersion corrected G06) were carried out by optimizing all the atomic positions, while keeping frozen the experimental unit-cell parameters (CASTEP software, version 19.11).[43] They were undertaken to characterize N_{Sac}•••Br and Br•••N_{Py} distances upon periodic conditions (Table 3).

Molecular calculations with complexes in gas-phase were conducted at the same level of theory than for monomers (PBEPBE-D2 aug-cc-pVTZ), either at the experimental frozen geometry or with optimization of the halogen atom position. Calculations at frozen experimental geometries (including the halogen atom) have been used to evaluate the electronic properties at the (3,−1) bond critical points (BCPs) of the $\rho(\mathbf{r})$-function,[39] as well as at the topological (3,−1)/(3,−3) CPs of the $L(\mathbf{r})$-function that correspond to atomic CD/CC sites in the valence shell of Br/N atoms, found in the internuclear N_{Sac}•••Br and Br•••N_{Py} regions (Table 3). Afterwards, the halogen atom position was optimized, keeping frozen the rest of the atoms. The theoretically calculated distances N_{Sac}•••Br and Br•••N_{Py} thus obtained are gathered in Table 3. Then, under the action of a homogenous electric field (ε) that was applied along the N_{Sac}•••N_{Py} direction, the Br-position between N_{Sac} and N_{Py} has been progressively shifted as a function of ε in the range $-40\times10^{-4} < \varepsilon < 100\times10^{-4}$ a.u. (1×10^{-2} a.u. = 5.1422082 GV/m). The electric field able to recover the experimental N_{Sac}•••Br and Br•••N_{Py} distances in the crystalline phase of the adduct, along with the corresponding integrated QTAIM net charges (Q) calculated for Br, and for the donor/acceptor fragments with Br belonging to one or another, are given in Table 3. The topological and energetic properties at BCPs of N_{Sac}•••Br and Br•••N_{Py}

interactions, along with the delocalization index (*DI*),[27] have been calculated as a function of ε and are gathered in Tables S1 to S4 (positive $\varepsilon > 0$ magnitudes are applied from N_{Sac} to N_{Py}). The electronic properties at the topological CPs of $\rho(\mathbf{r})$ and $L(\mathbf{r})$ functions have been calculated with the AIMAll software.[23]

In order to validate the choice of the methodology followed in this work (where complexes are frozen at experimental geometries while the Br-atom position is optimized upon the application of an external electric field), we have also fully optimized one of the adducts (NBrSac•••PyMe) while applying an external electric field ε in the same range of magnitudes explored in the manuscript and at the same level of theory (PBEPBE-D2 aug-cc-pVTZ) (Figures S7 and S8 and Table S5 in S.I.). Results show that whereas N_{Sac}•••Br and Br•••N_{Py} distances evolve qualitatively similar than in adducts frozen at experimental geometries except the Br-atom (N_{Sac}•••Br/Br•••N_{Py} distance increases/decreases with $\varepsilon > 0$, Figure S7), they cannot be quantitatively compared because the N_{Sac}•••N_{Py} distance also evolves with $\varepsilon > 0$ (Figure S7). Indeed, due to the absence of the rest of interactions with the omitted molecular environment around the adduct (not only polarization is involved), the N_{Sac}•••N_{Py} distance decreases then increases with increasing ε. However, normalizing the N_{Sac}•••Br and Br•••N_{Py} distances with respect to that of N_{Sac}•••N_{Py} along the range of applied fields, it shows that the evolving behavior of the normalized halogen bonding distances is very similar in both methods, in particular in the range of electric fields $\varepsilon \sim$ 50-80 x10^{-4} a.u. where experimental and Br-transfer geometries are found (Figure S8). Additionally, the angle between the N_{Sac}-Br bond vector and the NSacBr plane remains very close to that previously found along the full range of applied fields (the torsion angle C(SO2)-C(CO)-N-Br ranging respectively from -177.60° (ε = -20 x10^{-4} a.u.) to -179.35° (ε = 90 x10^{-4} a.u.) and from -177.33° (ε = -20 x10^{-4} a.u.) to -177.11° (ε = 80 x10^{-4} a.u.) in full optimized and frozen models). The N_{Sac}•••Br and Br•••N_{Py} distances that have been derived for the NBrSac•••PyMe adduct with the electric field balancing the electron properties |V|/G, ρ and DI at both halogen bonding interactions (the distances ranging respectively 2.069-2.076 Å and 2.102-2.095 Å with ε in the range 57 - 60.5 × 10^{-4} a.u., see Table 4) are reasonably close to those found with the full optimization of the adduct (respectively 2.084-2.120 Å and 2.167-2.136 Å, with ε in the range 50 - 60 × 10^{-4} a.u., at the PBEPBE-D2 aug-cc-pVTZ level of theory). Overall, these results indicate that a full geometry optimization of the adduct leads to a structural comparable behavior of the Br-atom position within the halogen bonding motif with respect to this found in the model where donor and acceptor moieties are frozen at

experimental geometries. Results concerning the full geometry optimization of the NsacBr•••PyMe adduct are gathered in Supplementary Information.

Acknowledgments.

We thank Université de Rennes for financial post-doctoral support (to I. N.) and CDIFX at ISCR for the use of X-ray diffractometers. This work has been supported by ANR (France) under contracts numbers ANR-17-CE07-0025-01 (Nancy) and ANR-17-CE07-0025-02 (Rennes). The EXPLOR mesocenter is thanked for providing access to their computing facility (project 2021CPMXX2483).

References

[1] Gilday, L. C.; Robinson, S. W.; Barendt, T. A.; Langton, M. J.; Mullaney, B. R.; Beer, P. D. Halogen Bonding in Supramolecular Chemistry. *Chem. Rev*. **2015**, *115,* 7118–7195.

[2] (a) Andrzejewski, M.; Olejniczak, A.; Katrusiak, A. Remote halogen switch of amine hydrophilicity. *CrystEngComm* **2012**, *14*, 6374−6376; (b) Aakeröy, C. B.; Beatty, A. M.; Lorimer, K. R. Charge-Assisted Hydrogen Bonds and Halogen-Halogen Interactions in Organic Salts: Benzylammonium Benzoates and Pentafluorobenzoates. *Struct. Chem.* **1999**, *10*, 229−242; (c) Aakeröy, C. B.; Spartz, C. L.; Dembowski, S.; Dwyre, S.; Desper. J. A systematic structural study of halogen bonding versus hydrogen bonding within competitive supramolecular systems. *IUCrJ* **2015**, *2*, 498–510.

[3] Simard, M.; Su, D.; Wuest, J. D. Use of hydrogen bonds to control molecular aggregation. Self-assembly of three-dimensional networks with large chambers. *J. Am. Chem. Soc.* **1991**, *113*, 4696−4998.

[4] Desiraju, G. R. Supramolecular Synthons in Crystal Engineering—A New Organic Synthesis. *Angew. Chem. Int. Ed. Engl*. **1995**, *34*, 2311–2327.

[5] (a) Corradi, E.; Meille, S. V.; Messina, M. T.; Metrangolo, P.; Resnati, G. Halogen Bonding versus Hydrogen Bonding in Driving Self-Assembly Processes Perfluorocarbon-hydrocarbon self-assembly, part IX. *Angew. Chem., Int. Ed*. **2000**, *39*, 1782−1786; (b) Aakeröy, C. B.; Fasulo, M.; Schultheiss, N.; Desper, J.; Moore, C. Structural Competition between Hydrogen Bonds and Halogen Bonds. *J. Am. Chem. Soc*. **2007**, *129*, 13772−13773; (c) Aakeröy, C. B.; Chopade, P. D.; Desper, J. Avoiding “Synthon

Crossover" in Crystal Engineering with Halogen Bonds and Hydrogen Bonds. *Cryst. Growth Des.* **2011**, *11*, 5333–5336; (d) Aakerôy, C. B.; Schlutheiss, N. C.; Rajbanshi, A.; Desper, J.; Moore, C. Supramolecular synthesis based on a combination of hydrogen and halogen bonds. *Cryst. Growth Des*. **2009**, *9*, 432–441.

[6] (a) Tothadi, S.; Desiraju, G. R. Designing ternary cocrystals with hydrogen bonds and halogen bonds. *Chem. Commun*. **2013**, *49*, 7791–7793; (b) Tothadi, S.; Sanphui, P.; Desiraju, G. R. Obtaining Synthon Modularity in Ternary Cocrystals with Hydrogen Bonds and Halogen Bonds. *Cryst. Growth Des*. **2014**, *14*, 5293–5302.

[7] Aakeröy, C. B. Is there any point in making co-crystals? *Acta Cryst.* **2015**, *B71*, 387–391.

[8] Aitipamula, S.; Banerjee, R.; Bansal, A. K.; Biradha, K.; Cheney, M. L.; Choudhury, A. R.; Desiraju, G. R.; Dikundwar, A. G.; Dubey, R.; Duggirala, N.; Ghogale, P. P.; Ghosh, S.; Goswami, P. K.; Goud, N. R.; Jetti, R. R. K. R.; Karpinski, P.; Kaushik, P.; Kumar, D.; Kumar, V.; Moulton, B.; Mukherjee, A.; Mukherjee, G.; Myerson, A. S.; Puri, V.; Ramanan, A.; Rajamannar, T.; Reddy, C. M.; Rodriguez-Hornedo, N.; Rogers, R. D.; Row, T. N. G.; Sanphui, P.; Shan, N.; Shete,G.; Singh, A.; Sun, C. C.; Swift, J. A.; Thaimattam, R.; Thakur, T. S.; Thaper, R. K.; Thomas, S. P.; Tothadi, S.; Vangala, V. R.; Variankaval, N.; Vishweshwar, P.; Weyna, D. R.; Zaworotko M. J. Polymorphs, Salts, and Cocrystals: What's in a Name? *Cryst. Growth Des*. **2012**, *12*, 2147–2152.

[9] Babu, N. J.; Sanphui, P.; Nangia, A. Crystal Engineering of Stable Temozolomide Cocrystals. *Chem. Asian J.* **2012**, *7*, 2274–2285.

[10] Aakeröy, C. B.; Fasulo, M. E.; Desper, J. Cocrystal or salt: does it really matter? *Mol. Pharm*. **2007**, *4*, 317–322.

[11] Makhotkina, O.; Lieffrig, J.; Jeannin, O.; Fourmigué, M.; Aubert, E.; Espinosa, E. Cocrystal or Salt: Solid State-Controlled Iodine Shift in Crystalline Halogen-Bonded Systems. *Cryst. Growth Des*. **2015**, *15*, 3464−3473.

[12] Dolenc, D.; Modec, M. EDA Complexes of N-halosaccharins with N- and O-donor ligands. *New J. Chem*. **2009**, *33*, 2344−2349.

[13] (a) Carlsson, A.-C. C. ; Uhrbom, M.; Karim, A.; Brath, U.; Gräfenstein, J.; Erdélyi, M. Solvent effects on halogen bond symmetry. *CrystEngComm* **2013**, *15*, 3087–3092; (b) Hakkert, S. B.; Erdelyi, M. J. Halogen bond symmetry: the N–X–N bond. *Phys. Org. Chem*. **2015**, *28*, 226–233; (c) Bedin, M; Karim, A.; Reitti, M.; Carlsson, A.-C. C.; Topić, F.; Cetina, M.; Pan, F.; Havel, V.; Al-Ameri, F.; Sindelar, V.; Rissanen, K.; Gräfenstein, J.; Erdélyi, M. Counterion influence on the N–I–N halogen bond. *Chem. Sci.*, **2015**, *6*, 3746–3756 and references therein.

[14] (a) Carlsson, A.-C. C.; Gräfenstein, J.; Budnjo, A.; Laurila, J. L.; Bergquist, J.; Karim, A.; Kleinmaier, R.; Brath, U.; Erdélyi, M. Symmetric Halogen Bonding Is Preferred in Solution. *J. Am. Chem. Soc*., **2012**, *134*, 5706–5715; (b) Carlsson, A.-C. C.; Gräfenstein, J.; Laurila, J. L.; Bergquist, J.; Erdélyi, M, Symmetry of $[N–X–N]^+$ halogen bonds in solution. *Chem. Commun*. **2012**, *48*, 1458-1460; (c) Lindblad, S.; Mehmeti, K.; Veiga, A. X.; Nekoueishahraki, B.; Gräfenstein, J.; Erdély, M. Halogen Bond Asymmetry in Solution. *J. Am. Chem. Soc*. **2018**, *140*, 13503–13513.

[15] Yu, S.; Truong, K.-N.; Siepmann, M.; Siiri, A.; Schumacher, C.; Ward J. S.; Rissanen, K. Halogen-Bonded $[N–I–N]^-$ Complexes with Symmetric or Asymmetric Three-Center–Four-Electron Bonds. *Cryst. Growth Des.* **2023**, *23*, 662−669.

[16] Rissanen, K.; Haukka, M. Halonium Ions as Halogen Bond Donors in the Solid State $[XL_2]Y$ Complexes. *Top. Curr. Chem*. **2015**, *359*, 77–90.

[17] Aubert, E.; Espinosa, E.; Nicolas, I.; Jeannin, O.; Fourmigué, M. Toward a reverse hierarchy of halogen bonding between bromine and iodine. *Faraday Trans*. **2017**, *203*, 389–406

[18] Puttreddy, R.; Mikko Rautiainen, J.; Makela, T.; Rissanen, K. Strong N−X···O−N Halogen Bonds: A Comprehensive Study on N-Halosaccharin Pyridine N-Oxide Complexes. *Angew. Chem. Int. Ed.* **2019**, *58*, 18610-18618.

[19] Laurence, C.; Graton, J.; Berthelot, M.; El Ghomari, M. J. The Diiodine Basicity Scale: Toward a General Halogen-Bond Basicity Scale. *Chem. Eur. J.* **2011**, *17*, 10431–10444.

[20] Brezgunova, M. E.; Aubert, E.; Dahaoui, S.; Fertey, P.; Lebegue, S.; Jelsch, C.; Angyan, J. G.; Espinosa, E. Charge Density Analysis and Topological Properties of Hal3-Synthons and Their Comparison with Competing Hydrogen Bonds. *Cryst. Growth Des*. **2012**, *12*, 5373−5386.

[21] Lamberts, K.; Handels, P.; Englert, U.; Aubert, E.; Espinosa, E. Stabilization of polyiodide chains via anion···anion interactions: experiment and theory. *CrystEngComm* **2016**, *18*, 3832−3841.

[22] Shukla, R.; Dhaka, A.; Aubert, E.; Vijayakumar-Syamala, V.; Jeannin, O.; Fourmigué, M.; Espinosa, E. Understanding Reactivity and Assembly of Dichalcogenides: Structural, Electrostatic Potential, and Topological Analyses of 3H-1,2-Benzodithiol-3-one and Selenium Analogs. *Cryst. Growth Des*. **2020**, *20*, 7704-7725.

[23] Keith, T. A. *AIMAll* (Version 19.10.12), TK Gristmill Software, Overland Park, Kansas, USA, **2019**

[24] Krawczuk, A.; Pérez, D.; Macchi, P. PolaBer: a program to calculate and visualize distributed atomic polarizabilities based on electron density partitioning. *J. Appl. Cryst.*, **2014**, *47*, 1452-1458.

[25] Mata, I.; Molins, E.; Alkorta, I.; Espinosa, E. Tuning the Interaction Energy of Hydrogen Bonds: The Effect of the Substituent. *J. Phys. Chem. A*, **2011**, *115*, 12561-12571.

[26] Mata, I.; Molins, E.; Alkorta, I.; Espinosa, E. Effect of an external electric field on the dissociation energy and the electron density properties: The case of the hydrogen bonded dimer HF···HF. *J. Chem. Phys*. **2009**, *130*, 044104.

[27] (a) Martín Pendás, A.; Blanco, M. A.; Francisco, E. Chemical Fragments in Real Space: Definitions, Properties, and Energetic Decompositions. *J. Comput. Chem*., **2007**, *28*, 161-184; (b) Outeiral, C., Vincent, M. A., Martín Pendás, A. and Popelier, P. L. A. Revitalizing the concept of bond order through delocalization measures in real space. *Chem. Sci*. **2018**, *9*, 5517–5529.

[28] Spackman, M. A.; Munshi, P.; Jayatilaka, D. The use of dipole lattice sums to estimate electric fields and dipole moment enhancement in molecular crystals. *Chem. Phys. Lett*. **2007**, *443*, 87−91.

[29] Kahn, R.; Cohen De Lara, E.; Möller, K. D. Effect of an electric field on a methane molecule. II. Calculation of the degeneracy splitting of the ν3 band. Expression of the second derivatives of the CH_4 dipole moment and evaluation of the second derivative of the C–H bond polarizability. *J. Chem. Phys*. **1985**, *83*, 2653−2660.

[30] Aubert, E.; Porcher, F.; Souhassou, M.; Lecomte, C. Electrostatic potential and interaction energies of molecular entities occluded in the AlPO4-15 molecular sieve: determination from X-ray charge density analysis. *J. Phys. Chem. Solids* **2004**, *65*, 1943−1949.

[31] Lehle, H.; Kriegl, J. M.; Nienhaus, K.; Deng, P.; Fengler, S.; Nienhaus, U. Probing Electric Fields in Protein Cavities by Using the Vibrational Stark Effect of Carbon Monoxide. *Biophys. J*. **2005**, *88*, 1978−1990.

[32] Suydam, I. T.; Snow, C. D.; Pande, V. S.; Boxer, S. G. Electric Fields at the Active Site of an Enzyme: Direct Comparison of Experiment with Theory. *Science* **2006**, *313*, 200−204.

[33] Espinosa, E.; Alkorta, I.; Elguero J.; Molins, E. From weak to strong interactions: A comprehensive analysis of the topological and energetic properties of the electron density distribution involving X–H···F–Y systems. *J. Chem. Phys*. **2002**, *117*, 5529-5542.

[34] Vijayakumar-Syamala, V.; Aubert, E.; Deutsch, M.; Wenger, E.; Dhaka, A.; Fourmigué, M.; Nespolo, M.; Espinosa, E. N-Iodosaccharin–pyridine co-crystal system under pressure: experimental evidence of reversible twinning. *Acta Cryst*. **2022**, *B78*, 436–449.

[35] Altomare, A.; Burla, M. C.; Camalli, M.; Cascarano, G.; Giacovazzo, C.; Guagliardi, A.; Moliterni, A. G. G.; Polidori G.; Spagna, R. SIR97: a new tool for crystal structure determination and refinement. *J. Appl. Cryst*., **1999**, *32*, 115-119.

[36] Sheldrick, G. M. A short history of SHELX. *Acta Crystallogr.*, **2008**, *A64*, 112-122.

[37] Farrugia, L. J. WinGX suite for small-molecule single-crystal crystallography. *J. Appl. Cryst*., **1999**, *32*, 837-838.

[38] Frisch, M. J., Trucks, G. W., Schlegel, H. B., Scuseria, G. E., Robb, M. A., Cheeseman, J. R., Scalmani, G., Barone, V., Mennucci, B., Petersson, G. A., Nakatsuji, H., Caricato, M., Li, X., Hratchian, H. P., Izmaylov, A. F., Bloino, J., Zheng, G., Sonnenberg, J. L., Hada, M., Ehara, M., Toyota, K., Fukuda, R., Hasegawa, J., Ishida, M., Nakajima, T., Honda, Y., Kitao, O., Nakai, H., Vreven, T., Montgomery, J. A. Jr, Peralta, J. E., Ogliaro, F., Bearpark, M., Heyd, J. J., Brothers, E., Kudin, K. N., Staroverov, V. N., Keith, T., Kobayashi, R., Normand, J., Raghavachari, K., Rendell, A., Burant, J. C., Iyengar, S. S., Tomasi, J., Cossi, M., Rega, N., Millam, J. M., Klene, M., Knox, J. E., Cross, J. B., Bakken, V., Adamo, C., Jaramillo, J., Gomperts, R., Stratmann, R. E., Yazyev, O. A., Austin, J., Cammi, R., Pomelli, C., Ochterski, J. W., Martin, R. L., Morokuma, K., Zakrzewski, V. G., Voth, G. A., Salvador, P., Dannenberg, J. J., Dapprich, S., Daniels, A. D., Farkas, O., Foresman, J. B., Ortiz, J. V., Cioslowski, J. & Fox, D. J. (2013). GAUSSIAN 09. Revision D. 01. Gaussian Inc., Wallingford, Connecticut, USA.

[39] Bader, R. F. W. Atoms in Molecules: A Quantum Theory; Oxford University Press: Oxford, **1990**.

[40] Bader, R. F. W.; MacDougall, P. J.; Lau, C. D. H. Bonded and nonbonded charge concentrations and their relation to molecular geometry and reactivity. *J. Am. Chem. Soc*. **1984**, *106*, 1594-1605.

[41] Bader, R. F. W.; MacDougall, P. J. Toward a theory of chemical reactivity based on the charge density. *J. Am. Chem. Soc*. **1985**, *107*, 6788-6795.

[42] Bader, R. F. W.; Gillespie, R. J.; MacDougall, P. J. A physical basis for the VSEPR model of molecular geometry. *J. Am. Chem. Soc*. **1988**, *110*, 7329-7336.

[43] Clark, S. J., Segall, M. D., Pickard, C. J., Hasnip, P. J., Probert, M. J., Refson, K. & Payne, M. C. *Z. Kristallogr*. **2005,** 220, 567–570.

For Table of Contents Use Only

Title: Atomic transfer in halogen-bonded complexes mediated by polarizing environments: Mimicking intra- and inter-molecular effects in a series of cocrystals of N-bromosaccharin with pyridines

Authors list: Emmanuel Aubert, Irène Nicolas, Olivier Jeannin, Marc Fourmigué and Enrique Espinosa

TOC graphic:

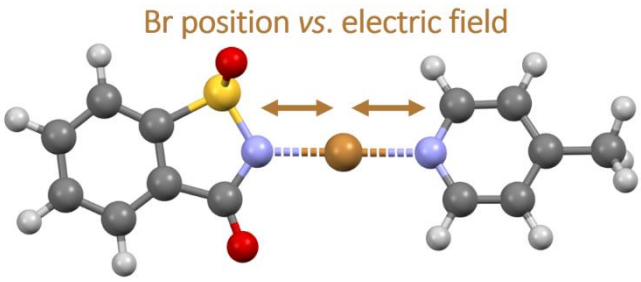

Synopsis: Shifting Br-atom position within donor-acceptor adducts by applying electric fields